

## 7. Final discussion and conclusions

Most of the world's seismicity, and nearly all of the earthquakes with magnitudes  $>8$ , are generated along convergent plate margins. To date, processes occurring along the plate interface of convergent plate margins (i.e. within a subduction channels) cannot be directly accessed by drilling nor through surface observations, but has been intensely studied with geophysical methods, numerical modeling, and sandbox simulations. However, these methods have either poor resolution, or are strongly dependent on insufficiently constrained assumptions. Hence, direct investigations of exhumed ancient convergent plate margins are requested to achieve insights into structures and processes which occurred along the plate interface. The here presented study contributes to the understanding of convergent plate margins in the depth range of their former seismogenic zone aiming at testing inferences and hypotheses of the various kinematic and mechanical concepts presented for the seismogenic zone. Therefore, we use the complete exposure of this part of a fossil plate interface in the European Alps, one of the best-studied mountain belts worldwide that has resulted from successive subduction, accretion and collision. Here, we analyzed a mélangé zone tracing the plate interface zone of the fossil convergent plate margin (Chapter 4). Additionally, we included information from Southern Chile, where material, which formerly underwent deformation along the plate interface, was exhumed to the surface by large scale accretion to the base of the upper plate (Chapter 1). We compare our field observation also with the assumptions from active convergent plate margins (Chapter 3). Therefore, the study is twofold, not even providing new aspects for the regional geology in the European Alps, but also providing constraints for inferences of structures and processes, which might be

subsequently tested at active convergent plate margins.

At first, we analyzed the South Penninic domain in the European Alps, which resulted from subduction of the Penninic oceanic domain underneath the Adriatic (Austroalpine) upper plate. Due to its comparability in lithofacies and internal structures to mélanges from subduction complexes (Ring et al. 1990) we treat the South Penninic domain as a subduction mélangé, which resembles material from a so-called subduction channel. The thickness of the South Penninic subduction mélangé varies from a few tens of meters up to more than 2500 m, reflecting their original thickness or a reduction from subsequent thinning. The matrix of shales and serpentinites incorporates clasts of more competent material, originating either from the Austroalpine upper plate (crystalline basement, its sedimentary cover), or formed by slivers of the lower plate (metagabbros, metabasalts, the sedimentary deposits of the ocean floor, or the trench fill turbidites). Therewith, it resembles the proposed internal structure of recently active subduction systems inferred from e.g. seismic and seismological data: less deformed units are bounded by a network of active shear zones or sheared matrix (e.g. Ábalos et al. 2003).

The South Penninic subduction mélangé exhibits a N-S gradient in metamorphic grade. In the northern part of the working area, Alpine metamorphism did not exceed diagenetic grades, or lower greenschist facies (Chapters 4, 6). In the southern part, rocks of the mélangé as well as the basal parts of the Austroalpine nappe stack were metamorphosed at middle to upper greenschist-facies conditions during Alpine orogeny. Due to large scale differential post-subduction tilting and exhumation of the fossil plate interface zone formerly deeper parts are accessible towards the south.

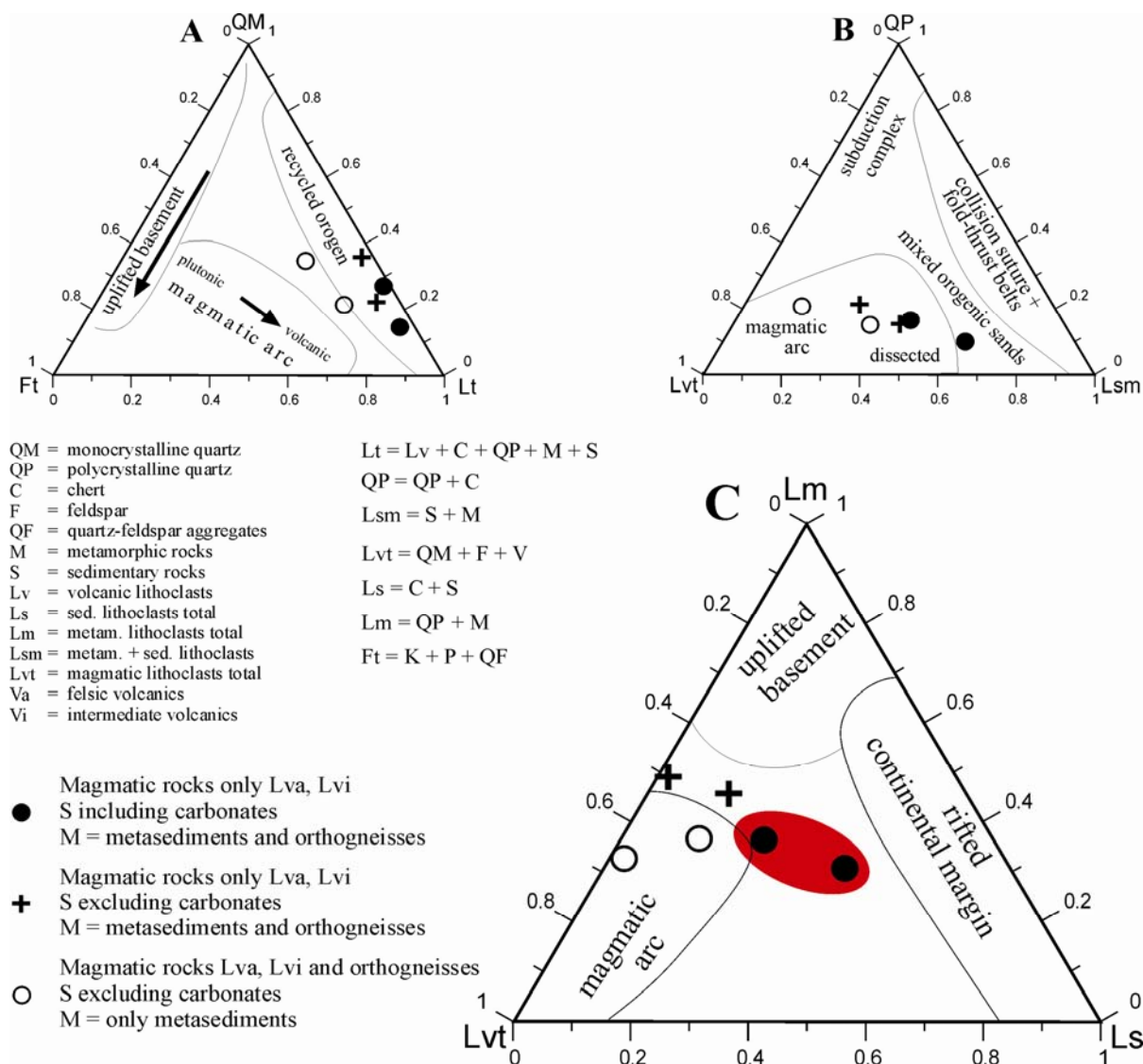


Fig. 7.1. Discrimination diagrams used for provenance analyses, based on Dickinson and Suczek (1979), Graham et al. (1993), and Ingersoll and Suczek (1979). Red shaded area denotes most reliable sample discrimination.

To better constrain the composition and the tectonic background of the subducted material in the study area, we applied provenance analyses to two samples from very-low grade sediment layers (profile 2). The discrimination diagrams (Fig. 7.1) show that the lithoclasts of both samples mainly consist of exhumed rock material of older orogenic origin. Metamorphic fragments with greenschist degree of overprint are thought to represent the dissected magmatic arc of the Paleozoic basement. In addition, 25% to 40% of the material is of magmatic-arc input. Because

of dominating rhyolitic fragments, it presumably may be related to Jurassic rifting. The high degree of recrystallized glassy matrix of these fragments rather excludes derivation from the Tertiary magmatic arc. Carbonatic fragments may derive either from Cretaceous basin sediments associated with rifting, which started in Middle Jurassic times (Ring et al. 1989; von Eynatten and Gaupp 1999), or to the Triassic cover of the basement prior to the onset of rifting processes. Due to the abundance of variegated components, minor tectonic and metamorphic overprint,

as well as the low degree of the component's rounding (subangular to subrounded) we conclude that the studied sediments are derived from the sedimentary cover of the South Penninic ocean. They might represent proximal turbiditic greywackes, which have been subducted to shallow depths and later accreted to the base of the overlying Austroalpine nappe stack.

The material comprising the fossil subduction channel is comparable to material thought to be subducted at recently active convergent plate margins (Chapter 3). According to Hashimoto et al. (2006), this material should be composed of clay mineral, trench-filling sand and carbonates. Also, the extension of sandstone blocks and layers, as proposed by these authors, is well visible throughout the study area (Chapter 4). In consequence, the exposed fossil subduction plate interface zone resembles active plate interface zones, despite of overprint during collision and exhumation, at least in terms of its compositional setup. We propose that in addition to the comparable composition, the behavior of the fossil plate interface zone was equivalent to recently active systems in terms of stable, unstable and conditional stable areas, as this is governed by the divers sediment input over time (Chapters 4, 5). Even spatiotemporal varying mass transfer mode is similar to presently active systems (Chapter 6).

We restored the fossil plate interface zone in the Swiss Alps to its former subduction geometry resulting in a 170 km long section with a ca.  $8^\circ$  SSE-dipping plate interface for the Late Cretaceous to Eocene period, prior to collision and underplating of the continental Briançonnais domain. This restoration does not provide hints for a major overprint of the pattern of subduction-related metamorphism by younger events. All later offsets visible within the section from Schmid et al. (1996) are below 1 km, except for the

oblique-slip Engadine line (Chapter 4). This is also in agreement with our field observations missing a penetrative overprint of the general top-W directed tectonic transport. Nevertheless, the present day fossil subduction channel has been influenced by post-subduction and post-accretion processes during ongoing convergence between both plates. These processes may have involved either both the South Penninic domain and the Austroalpine nappe stack, or only reactivated the direct contact between the lower and the upper plate. Magnitudes of subsequent deformation are small with respect to the total length and minimum displacement along the plate interface, and may even largely cancel out. The here calculated dip angle of the plate interface ( $\sim 8^\circ$ ) is in good agreement with published average megathrust angles (Lallemand et al., 1994; Moores and Twiss, 1995; Clift and Vannucchi, 2004). Therefore, we consider later modifications irrelevant at the here applied scale of observation.

In contrast to the compositional homogeneity in all studied transects, other features show a characteristic downdip change: the overprint of the upper plate base by Alpine deformation increases towards depth (respectively towards the south of the working area), the matrix of the subduction channel exhibits an equally increasing deformation and metamorphic grade, and the number of mylonitic shear zones and mylonitic rocks progressively increases as well. The density of LDZ also increases downdip ultimately involving the entire subduction channel matrix (Fig. 7.2). Because of more or less continuous flux of material in the subduction channel, all features will be displaced downdip once formed, or even updip due to return flow. This will result in (1) an offset of mélange features with regard to the overlying features at the base of the upper plate (except for first occurrence of features); (2) an apparent downdip increase in key features; and (3) apparently gradational

boundaries that may have been more distinct during formation. However, none of these aspects will be of significance in the upper plate. There, spatial and temporal varying frictional conditions within the plate interface zone caused by spatiotemporal variable sediment input might additionally smear out distinct boundaries for the onset of plate interface key features (e.g. pseudotachylytes formed within the basal parts of the crystalline upper plate resulting from frictional instability within the subduction channel). In consequence, the plate interface zone cannot exhibit a steady state behavior.

We interpret the occurrence of pseudotachylytes along the exhumed plate interface as delineating the area of unstable slip within the ancient subduction channel (Chapter 4) (Fig. 7.2). The fossil updip limit of unstable slip is located at a distance of ~90 km from the trench corresponding to a depth of ~15 km, and a temperature of ~200°C (Fig. 7.2). The fossil downdip limit of unstable slip is located at a distance of 140 km from the trench equivalent to a depth of ~22 km, and a temperature of ~300°C (Fig. 7.2). The conditionally stable segments above and below the unstable segment may continue for some distance updip and downdip. Below the downdip end of unstable slip we observe a continuing increase of LDZ in the *mélange* that may be seismic, jointly occurring with mylonites (Chapter 4). Therefore, we postulated seismic behavior to be possible in the subduction *mélange* to temperatures of at least 300°C to 350°C and possibly higher. However, formation of LDZ and associated seismic behavior is strongly lithology dependent (Chapter 4). The mylonitic overprint of pseudotachylytes, the mutual crosscutting of overprinted and non-overprinted pseudotachylytes, the drastic increase in LDZ, and the onset of mylonitic rocks in the subduction *mélange* and, slightly deeper, at the base of the upper plate, point to the coincidence of the

downdip limit of unstable slip with the start of a transitional zone at the downdip limit of the seismogenic coupling zone.

The updip extent of the fossil seismogenic coupling zone is proposed to be much wider than outlined by the zone of unstable slip, because the here estimated updip limit of unstable slip (~15 km depth, 200°C) is below the widely accepted values for active convergent plate margins (~5 km depth, 100°C-150°C, e.g. Oleskevich et al., 1999). Additionally, we observed localized deformation zones trenchward of the estimated upper limit of the unstable slip area. Otherwise, pressure solution seams, which are widespread in the northern part of the working area, are evidence for aseismic creep (e.g. Kitamura et al., 2005), possibly prevailing in the postseismic relaxation period.

Evidence for fluids circulating along the plate interface are widespread in the study area: foliation-parallel blocky-textured mineralized veins in the *mélange* matrix, veins cutting into competent clasts both downdip of profile 4 (Chapter 4), solution-precipitation creep as dominant deformation mechanism in all of the study area, dehydration reactions in the *mélange* matrix, and hydration as well as sealing of the upper plate base. Fluid percolation must have occurred unimpeded through a permeable fracture network, along foliation planes and grain boundaries in the upper conditionally stable domain because of the absence of mineralized veins updip of profile 4 (Fig. 7.2). Starting in the unstable slip area, formation of mineralized veins clearly requires fluid production rate to exceed percolation rate building near-lithostatic fluid pressure during parts of the seismic cycle. The internal structure of the mineralized veins resembles the structure of pseudotachylyte networks. Embedded wall rock fragments within the mineralized veins and within the pseudotachylytes - either with or without minor contact to the wall rock - point to fast fracturing and

subsequent rapid solidification processes. From the spatial coincidence of both features and their identical texture we postulate that formation of the mineralized veins potentially indicates unstable slip in the subduction *mélange*. The exclusive restriction of pseudotachylytes and mineralized vein systems to one component of the plate boundary system - i.e. base of upper plate vs. *mélange* - is most likely due to a different rheological behavior of the subduction *mélange*, and the crystalline basement of the upper plate.

Additionally, we observed blocky-textured mineralized veins, which are aligned sub-parallel to the overall foliation, in both metasediments and metabasic rocks in our second working area in Southern Chile (Chapter 1.3.2.). They are identical in texture and occurrence compared to the observed mineralized veins within the European Alps. However, according to PT estimates by Glodny et al. (2005) they have been formed deeper along the plate interface zone (8-9 kbar in Southern Chile). This also indicates proceeding vein formation along the plate interface, deeper down as observable in the European Alps. Its geometric style changes deeper down with longer and wider veins, still indicating ongoing hydrofracturing in the lower conditionally stable zone, as also observed for the LDZ. The heterogeneous internal structure of the subduction *mélange* governs the transport of released fluids both along and across the foliation, foliation parallel shear planes, and thus, the plate interface.

The transition between seismic and aseismic deformation in our studied example is well comparable to the proposed transitional zone downdip of the seismogenic part of active convergent plate interfaces (e.g. Hyndman and Wang, 1995). There, seismic slip in the transitional zone may occur during major coseismic events rupturing the entire unstable slip zone, subsequently

overprinted by viscous deformation during postseismic relaxation and interseismic creep. However, we note that our observations of proceeding vein formation, formation of LDZ, and the viscous overprint of brittle structures in the lower conditionally stable segment (Fig. 7.2) might also be indicators for a domain of slow earthquakes (slow slip events) and associated non-volcanic tremors, as proposed for many active subduction zones in a comparable depth range (e.g. Schwartz and Rokosky 2007).

We analyzed Sr isotope signatures of marine (meta-) carbonates. They are shown to be governed by both depositional and syn-subduction recrystallization history. Metamorphosed carbonate samples from the subduction *mélange* exhibit clear evidence for syn-metamorphic alteration by fluids. Increased  $^{87}\text{Sr}/^{86}\text{Sr}$  ratios of the metacarbonates indicate devolatilization of old continental crustal material as dominant source of syn-subduction fluids, probably of subducted continental detritus. This is in line with the prediction by e.g. Moore and Saffer (2001) highlighting the fluid production potential of subducted sediments at active subduction zones (Chapter 3) (Fig. 7.2) Subduction fluids from other sources, like dehydration of oceanic crust (e.g. Peacock 2000, Chapter 3), cannot be ruled out, but must have been minor due to the low  $^{87}\text{Sr}/^{86}\text{Sr}$  ratios expected for such fluids, which is in strong contrast with the compositions observed in the subduction *mélange* samples.

To determine the absolute timing of subduction-related deformation (Chapter 6), we used Rb/Sr geochronology on pervasively deformed rocks from both the South Penninic subduction *mélange* and the Austroalpine upper plate. Results of Rb/Sr isotope analyses shed light on the pre-Alpine and Alpine deformation history along the suture. The deformational and isotopic record of a subduction channel is persistently renewed due to continuous

processes such as sediment subduction and tectonic erosion. Only when material finally left the active parts of the subduction channel and became accreted to the base of the hanging wall, the deformational and isotopic record can be preserved. Deformation induced isotopic resetting during accretion of material to the base of the upper plate is caused by permanent strain accumulation due to velocity gradient between material flow within the channel and the upper plate. Due to a missing overprint of the isotopic system by later deformation events, our Rb/Sr isotopic ages date the removal of material out of the active parts of the subduction channel and the abandonment of the South Penninic-Austroalpine suture zone at roughly 50 Ma (Fig. 7.2). Rb/Sr ages are identical for pervasively deformed Austroalpine and South Penninic rocks. Metamorphic mobilisate, which is dated to 50 Ma, points to syn-subductional dehydration, fluid activity and mineral precipitation. According to our structural data, the latest increment of subduction-related deformation (at ~50 Ma) is characterized by a roughly top-W direction of tectonic transport.

Referring to published paleogeographic reconstructions, the end of subduction-related deformation is best explained by the locking of the South Penninic paleosubduction interface due to underplating of the Middle Penninic micro-continent, a process that caused a relocation of convergence-related strain from the paleosubduction *mélange* into the new, Middle Penninic footwall. The shutoff of sedimentation in the forearc Gosau basins is contemporaneous with basal accretion of the South Penninic *mélange* and the Middle Penninic units, both processes occurring in the Lower Eocene (~50 Ma). We therefore hypothesize a causal link between the two events, with the change from tectonic erosion to basal accretion being responsible for a regional pulse of uplift,

leading to inversion of the forearc basins. Von Blanckenburg and Davies (1995) suggest the underplating of continental Penninic material (most likely the Middle Penninic micro-continent) below the overriding plate in a time span between 55 Ma and 45 Ma (Fig. 6.12b). Our Rb/Sr age data are in line with these suggestions.

Rb/Sr deformation ages additionally have the potential to constrain the mode of syn-subduction interplate mass transfer. Hypothetical endmember scenarios for such mass transfer modes within subduction channels (Chapter 6) would result in: 1) continuous underplating adding material to the base of the upper plate (basal accretion), 2) continuous tectonic erosion removing material from the base of the upper plate, or 3) steady state continuous material flow neither adding nor removing material. Nearly identical Rb/Sr ages for pervasively deformed Austroalpine and South Penninic rocks point to tectonic erosion of the upper plate during subduction. This is also evidenced by the lack of upper plate crystalline basement immediately above the plate interface in some parts of the working area where upper plate sediments directly rest on the *mélange*, by the presence of upper plate clasts in the subduction *mélange* (e.g. Oncken 1998, Chapter 4), and from the syn-subduction evolution of Gosau forearc basins pointing to tectonic erosion as prevailing mass transfer mode during the time of subduction. Basal subduction erosion invariably stopped upon underplating of the *mélange*, and abandonment of the subduction of the South Penninic ocean. Lack of a metamorphic contrast between the South Penninic *mélange* and the Austroalpine upper plate favors exhumation of the suture zone due to a combination of tectonic underplating and surface erosion.

Another part of the study was  $^{40}\text{Ar}/^{39}\text{Ar}$  geochronology on pseudotachylytes to

constrain the timing of occurrence of unstable slip (Chapter 5). Defocused beam microprobe bulk analyses of the pseudotachylyte groundmass point to a mixture of amphibole, feldspar and possibly biotite, which equal the paragenesis of the host rocks. In addition, rock fragments and single minerals from the host rock of comparable size are incorporated in the pseudotachylyte groundmass. They provide a source for inherited argon, and thus complicating the interpretation of the isotopic data. We omitted visible wall rock fragments and single crystals inherited from the host rocks, but we cannot argue for a complete leave out of distracting inclusions. The use of a laser system in order to degas Ar by stepwise heating resulted in a rather localized heating of the sample. Despite of the small spot size, we expect the degassing of Ar to occur from a mixture of the ultra fine grained newly crystallized lasts and from wall rock fragments and single crystals, rather than from a homogeneous solidified melt. Our obtained  $^{40}\text{Ar}/^{39}\text{Ar}$  ages, as erroneous they might be, point to unstable slip and therewith associated pseudotachylyte formation within the basal parts of the Austroalpine nappe stack during a prolonged time span between 60 Ma to roughly 80 Ma (Fig. 7.2). The data of Thöni (1981, 1988) fall into the bracketed time frame. Due to the temporal similarity between subduction and pseudotachylyte formation, and the fact that the pseudotachylytes occur subparallel to the main thrust where Austroalpine rocks were overthrust onto South Penninic rocks, we interpret the generation of pseudotachylytes to be related to unstable slip processes occurring along the plate interface zone during subduction of the South Penninic ocean underneath the Austroalpine upper plate (Chapter 5).

The slightly difference between our Rb/Sr deformation ages for the southern parts of the working area (~50 Ma), and the

$^{40}\text{Ar}/^{39}\text{Ar}$  ages for pseudotachylyte formation within the central part of the working area (80 Ma to 60 Ma) might be either caused by methodological limitations or by changes in the mass transfer mode. While using Rb/Sr isotopic data we dated last increments of deformation induced resetting, and thus the end of a deformation process. The use of the Ar isotopic system constrain the obtained ages to a temperature sensitive degassing step during formation and recrystallization of the melt veins, which could be somewhat older than the last increment of deformation captured by the Rb/Sr system. Otherwise, the difference can also be explained by the incorporation of wall rock fragments and single minerals within the pseudotachylyte matrix leading the inherited argon, and thus to apparently too old ages. Additionally, according to our proposed endmember scenarios of material flux within the subduction channel, which we postulated to be elucidated using isotope geochronology, the difference in both geochronological methods could provide additional hints for spatiotemporal changes in tectonic erosion and accretion. Assuming tectonic erosion, the last increments of unstable slip might be erased from the base of the upper plate and transported towards depth, continuously shifting the area of isotopic resetting into the upper plate (Chapter 5). The mylonitization of pseudotachylytes at the immediate base of the upper plate might favor this explanation. Only geochronological studies of the mylonitic overprinted pseudotachylytes have the potential to finally answer this question.

The potential of this study is the possibility to draw direct connection from field-based observations to their proposed counterparts from active convergent plate margins. The distribution of earthquakes within the subduction channel as well as the basal part of the upper plate proposed for active subduction zones (Chapter 3) is comparable to the observed



Figure 7.2: Final interpretative section showing the profile positions (number in circles), as well as the association and interference of the observed key features. Areas of conditional stability occur above and below the unstable slip region, characterized by the coexistence of slow deformation and maybe seismic deformation (e.g. LDZ, mineralized veins). The regions of stable, conditional stable and unstable slip will vary in space and time in accordance to spatiotemporal variance in e.g. sediment input, dewatering and dehydration. Thus, the mechanical conditions within the subduction channel are not characterized by steady state behaviour. Model of frictional conditions modified and extended downdip following Bilek and Lay (2002). Results of Rb/Sr and  $^{40}\text{Ar}/^{39}\text{Ar}$  geochronology are indicated. Additionally, we summarized key observations from recently active convergent plate interfaces. See text for details.

pseudotachylytes along the base of the Austroalpine upper plate, and the potentially seismicity-indicating mineralized veins and LDZ within the subduction mélangé (Fig. 7.2). The reported increase in seismic reflectivity towards depth (until a certain threshold) from active subduction zones (e.g. Oncken et al. 1999, Calvert et al. 2003) might be due to the increase in fabric development (foliation planes, shear zones, mineralized vein systems) observable at the fossil counterpart, in line with the prediction from active systems (Fig. 7.2). The broad reflector downdip the Cascadian subduction zone is interpreted to be related to mylonitic rocks in the temperature range between 250°C to 350°C (e.g. Nedimovic et al. 2003). In a comparable depth range with our fossil analogue we observed the increase in deformation, progressively involving the whole subduction channel (metasedimentary rocks intermingled with slivers of both oceanic and continental origin) and basal parts of the upper plate (Fig. 7.2). This might provide a structural evidence for the observed broad zone of reflectivity (e.g. Nedimovic et al. 2003 for Cascadia). Trapped fluids causing reflectivity e.g. along the Chilean subduction zone (e.g. Krawczyk et al. 2003) are widespread downdip the fossil plate interface, forming partly lentoid bodies. Furthermore, the low velocity zone being interpreted as a subduction channel (Krawczyk et al. 2006, and references therein) might be caused by the mixture of subducted sediments (with low  $V_P$  values)

with material from the upper and the lower plate – a composition equally to the observations with the fossil counterparts (Fig. 7.2). The observed intermingling of metasediments and slivers of upper and lower plate origin was also postulated by Calvert (2004) to be responsible for the observed  $V_P$  values (Chapter 3). High  $V_P/V_S$  ratios along the plate interface zone are assumed to be indicators for the presence of water saturated sediments (Husen et al. 2000), also in line with our field observations showing ubiquitous evidence for subducted sediments and dewatering and dehydration reactions, as well as fluid circulation.

Finally, the plate interfaces of the studied fossil convergent plate margins experienced flow and fracturing over an extended period of time reflecting a multistage evolution (especially the European Alps), but resemble active convergent plate margins in terms of e.g. sediment input, earthquake distribution, fluid circulation, and possible slow slip events and associated tremors. We suggest the testing of our field-based subduction plate interface setup with synthetic seismograms in order to prove the resolvability of the observed structures and lithological contrasts (i.e. clasts, duplexes). This would finally help to better constrain synthetic geophysical, numerical and analogue modelling, and offers the chance for a more detailed identification of processes within ancient and active subduction channels.

